Linearization of Euclidean norm dependent inequalities applied to multibeam satellites design

Jean-Thomas Camino, Christian Artigues, Laurent Houssin, Stéphane Mourgues

Noname manuscript No.
(will be inserted by the editor)

Linearization of Euclidean Norm Dependent Inequalities Applied to Multibeam Satellites Design

Jean-Thomas Camino · Christian Artigues · Laurent Houssin · Stéphane Mourgues

Received: date / Accepted: date

Abstract Euclidean norm computations over continuous variables appear naturally in the constraints or in the objective of many problems in the optimization literature, possibly defining non-convex feasible regions or cost functions. When some other variables have discrete domains, it positions the problem in the challenging Mixed Integer Nonlinear Programming (MINLP) class. For any MINLP where the nonlinearity is only present in the form of inequality constraints involving the Euclidean norm, we propose in this article an efficient methodology for linearizing the optimization problem at the cost of entirely controllable approximations even for non convex constraints. They make it possible to rely fully on Mixed Integer Linear Programming and all its strengths. We first empirically compare this linearization approach with a previously proposed linearization approach of the literature on the continuous $k-$center problem. This methodology is then successfully applied to a critical problem in the telecommunication satellite industry: the optimization of the beam layouts in multibeam satellite systems. We provide a proof of the NP-hardness of this very problem along with experiments on a realistic reference scenario.

Keywords Mixed Integer Linear Programming · Mixed Integer Nonlinear Programming · Euclidean Norm Linearization · $k-$center problem · Multibeam Satellites

Jean-Thomas Camino
LAAS-CNRS, Université de Toulouse, CNRS, UPS, Toulouse, France
Airbus Defence and Space, Space Systems, Telecommunication Systems Department, Toulouse, France

Christian Artigues · Laurent Houssin
LAAS-CNRS, Université de Toulouse, CNRS, UPS, Toulouse, France
E-mail: laurent.houssin@laas.fr

Stéphane Mourgues
Airbus Defence and Space, Space Systems, Telecommunication Systems Department, Toulouse, France

1 Introduction

In the wide literature on mathematical optimization, there are several examples of problems involving continuous point variables in $\mathbb{R}^2$ or $\mathbb{R}^3$ with constraints on the Euclidean distance between pairs of such points. In some of these problems, the possibility to rely on convex optimization is preserved: for instance, an upper-bound on a Euclidean distance between two points is a convex constraint. On the other hand, any equality or lower-bound set on a Euclidean distance makes the corresponding optimization problem non-convex. In any case though, these quadratic constraints position the optimization in the Nonlinear Programming (NLP) class. More details on Euclidean distance geometry and applications can be found in [15] and [1] but one of the most famous problems that handles such 2-norm computations over continuous variables is the Euclidean Multifacility Location Problem (EMFL): [27], [26]. This problem consists in defining positions for n new facilities with respect to m existing facilities. The minimized cost function terms are proportional to distances between pairs of new facilities, and to pairwise distances between old and new facilities. Most algorithms that solve the EMFL rely on second-order cone programming and interior point techniques for convex optimization since the problem can be equivalently transformed into another one where convex quadratic proximity constraints appear.

For works that consider both proximity and separation constraints, we can mention for instance the research on wireless sensor localization (see [17] for a thorough survey on the matter). In this problem, we assume that a set of sensors has been deployed on a certain region, and that some of the sensor positions are known while the others are not, the goal being to estimate these unknown positions. The authors of [3] have indeed to deal with non-convex equality and separation constraints which they choose to relax just enough to reach a semidefinite programming model. In some cases, discrete variables are necessary to model decisions with finite numbers of possibilities. When combined with the Euclidean norm constraints discussed above, these integer variables lead to Mixed Integer Nonlinear Programming (MINLP), which is known to be one of the most difficult optimization problems class ever to be tackled. As an example of such problems, the authors of [25] worked on the issue of packing unequal spheres in a 3-dimensional polytope with sphere separation constraints and an objective to maximize the volume occupied by the spheres, the application being radiosurgical treatment planning. In that case, the continuous variables are the sphere centers, and the discrete variables correspond for each sphere to the choice of a radius among a finite set of possibilities. This non-convex quadratic problem is solved with an heuristically improved simplicial branch-and-bound method.

Another example in the satellite industry is the problem of optimizing the beam layouts of a multibeam telecommunication satellite system (see [5], [6] and [14] for instance). It consists of defining the positions in the Euclidean plane of a certain number of disks, each one representing the spatial extent of a radiofrequency beam that carries telecommunication signals for various applications: television, telephone, radio or internet by satellite for instance. While the number of user ground stations (modeled by points of known coordinates in the Euclidean plane) covered by these disks of discretely varying diameter is maximized, satellite antenna technological

constraints force some couples of disks to be sufficiently separated. Note that this last application is the one that motivated this work.

In the end, the focus of this article is laid on the particular MINLP problems where the only nonlinearities are quadratic constraints expressed with an Euclidean distance over continuous variables. Both separation and proximity constraints are handled, and they cohabit with discrete variables, in order to optimize a linear objective. For these problems, we detail in section 2 the methodology we devised for reaching a Mixed Integer Linear Programming model (MILP) thanks to controllable approximations, the goal being to take full advantage of all the efficient techniques developed for this specific class of optimization problems. In section 3, we show that the family of controllable approximations we propose both generalizes and ease the linearization of previously proposed approximations. A comparison of the proposed MILP with another linearization scheme of the Euclidean distance is carried out with computational experiments on the continuous k-center problem in section 4. In section 5, the beam layout optimization is defined more in details, its NP-hardness is proven, and the principles of section 2 are applied in order to reach a MILP model which is presented and commented. A comparison with other linearizations and experiments on a reference scenario are presented in section 6. Concluding remarks are drawn in section 7.

2 Linearization of Euclidean norm dependent constraints in $\mathbb{R}^2$

Let $X \in \mathbb{R}^2$ and $\alpha, \beta \in \mathbb{R}^+$. We develop in this section a MILP-compatible linearization process of the constraints of the following form: $\|X\| \leq \alpha$ and $\|X\| \geq \beta$ with $\|\cdot\|$ denoting the Euclidean norm. The associated inner product will be denoted by $\langle \cdot \mid \cdot \rangle$. The choice of $\mathbb{R}^2$ is directly motivated by the beam layout optimization application, but the principles presented could be generalized to $\mathbb{R}^3$, or to higher dimensions. Also note that, even if it is not discussed here, these techniques could also be extended to the constraints of the form $\|X_1\| + \cdots + \|X_k\| \leq \alpha$ and $\|X_1\| + \cdots + \|X_k\| \geq \beta$ with $k > 1$.

On the topic of linearizing the Euclidean norm in the context of mathematical optimization, the examples are rare but can be found in the applications overviewed of section 1. In the context of radiotherapy equipment configuration, the authors of [16] propose to linearize the quadratic terms of the convex proximity constraints with extra variables and a notion of approximation points, but without really discussing the error made in the end on the approximated Euclidean distances. Another way of linearizing the Euclidean distances is to discretize the possible positions of the originally continuous variables allowing then to pre-compute all the possible point-to-point distances, as done both in [16] and [5]. Although, our ambition in this work was to preserve this continuity of the position variables so this type of discretization has been discarded. Then, in the context of wireless sensor location, the author of [11] approximates the Euclidean distances by the L_1 norm and exploits the triangle inequality for reaching a linear programming model. This last technique falls

within a more general wave of research in the field of digital distances on how to substitute cleverly the computationally expensive L_2 norm calculations by optimized combinations of the less demanding operation L_1 and L_∞ norms. Note also that these two norms are much more naturally linearizable norms than the Euclidean norm. The most recent works ([7], [19]) on the subject showed that in the Euclidean plane, the best maximum relative error of an optimized combination of the L_1 and L_∞ norms with respect to the L_2 norm is approximately equal to 5.6%. In the same paper the best combination of an overestimating norm, the euclidean Chamfering weighted distance in 2-D, and an underestimated norm, the Inverse square root weighted t-cost distance in 2-D provide the best empirical MRE of 1.29%. There are two issues with such linear combination of overestimating and underestimating norms. First, the resulting norm is neither an over-approximation nor an under-approximation of the euclidean norm. However, as we aim at modeling minimum or maximum distance constraints in industrial optimization problems, the linear combinations do not allow a strict enforcement of such constraints. In [19], exact MREs of such norms were provided. The MRE of the best overestimating norm is about 8.24 %, while the MRE of the best underestimating norm is about 7.61%. The second issue is that we are looking for a totally controllable approximation of the Euclidean norm whose maximum relative error could tend towards 0 if one was willing to pay the price in terms of numerical complexity. The polyhedral $\varepsilon-$approximation approach by [2, 12] answers partially this requirement for convex second order cone constraints, which can express upper bound on Euclidean distance. In this spirit, we propose a family of polyhedral approximations of the Euclidean distance based on uniform plane directions discretization that also allows to tackle lower bound constraints on the Euclidean distance, which are non convex constraints. We will also show that this family of approximations both generalizes and makes easier the linearization of the above referenced under- and over-approximations.

2.1 Euclidean norm linearization through uniform plane directions discretization

To find such a convenient linearization process, we relied on two geometrical results. They are both based on a parametrically controlled discretization of the directions of the Euclidean plane, that are otherwise characterized by the continuous domain $[0, 2\pi[$. In practice, for a given $n_{\text{directions}} \in \mathbb{N}$ such that $n_{\text{directions}} \geq 3$, and for all $i \in \{1, \cdots, n_{\text{directions}}\} = \mathcal{U}$, let us denote by

$$U_i = \begin{pmatrix} U_{i,x} \\ U_{i,y} \end{pmatrix} = \begin{pmatrix} \cos\left(\dfrac{2(i-1)\pi}{n_{\text{directions}}}\right) \\ \sin\left(\dfrac{2(i-1)\pi}{n_{\text{directions}}}\right) \end{pmatrix} \in \mathbb{R}^2 \tag{1}$$

the i^{th} discretized direction (running notation throughout the paper). These $n_{\text{directions}}$-th roots of unity provide a uniform discretization of the Euclidean plane directions with each resulting direction representing an exclusive sub-interval of $[0, 2\pi[$ of size $\frac{2\pi}{n_{\text{directions}}}$. See for instance Fig. 1(a) for an example with 8 directions. Note that by

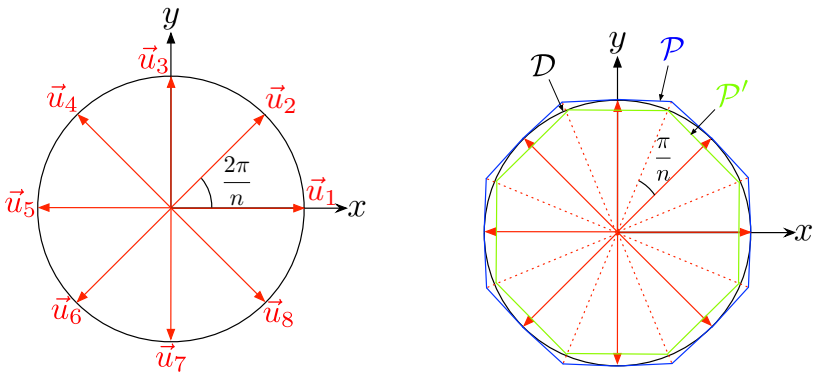

Fig. 1 (a) Uniform discretization of the directions of the Euclidean plane ($n_{\text{directions}} = 8$) : the 8^{th} roots of unity (b) Approximation of the Euclidean plane disk $\mathcal{D}$ by the regular $n_{\text{directions}}$-sided polygons $\mathcal{P}$ and $\mathcal{P}'$ with the linear approximation of the Euclidean norm

definition, we have:

$$\forall i \in \mathcal{U}, \quad \|U_i\| = 1 \tag{2}$$

In practice, the *Proposition* 1 presented below allows to define a process based on linear operations to check whether two points $u, v \in \mathbb{R}^2$ are closer than a given distance: one has to check that the projections of the $u - v$ vector on the U_i directions are all lower than a precise threshold. The fact that u and v will be decision variables (position variables) while the U_i directions will be input data is to be kept in mind to understand the linearity of the process proposed.

Proposition 1 *Let $u, v \in \mathbb{R}^2$ and let $d \in \mathbb{R}^+$,*

$$[\ \forall i \in \mathcal{U},\ \langle u - v \mid U_i \rangle \leq d\ ] \Longrightarrow \|u - v\| \leq \frac{d}{\cos(\theta_{max})} \tag{3}$$

where $\theta_{max} = \dfrac{\pi}{n_{directions}}$

Proof Let us therefore assume that

$$\forall i \in \mathcal{U}, \quad \langle u - v \mid U_i \rangle \leq d \tag{4}$$

Since two consecutive directions are separated by an angle of exactly $\frac{2\pi}{n_{\text{directions}}}$, we necessarily have the following constraint on the angle $\angle(u - v, U_{i_{\min}})$

$$\angle(u - v, U_{i_{\min}}) \leq \frac{\pi}{n_{\text{directions}}} = \theta_{\max} \tag{5}$$

where the direction $i_{\min} \in \mathcal{U}$ is defined as the closest direction to $u-v$ in terms of angular separation. Therefore, since $||U_{i_{\min}}|| = 1$ and since $\theta_{\max} \in [0, \frac{\pi}{3}]$:

$$\cos(\theta_{\max}) \|u-v\| \leq \langle u-v \ , \ U_{i_{\min}} \rangle \tag{6}$$

and since $i_{\min} \in \mathcal{U}$ and therefore verifies the equation (4):

$$\|u-v\| \leq \frac{d}{\cos(\theta_{\max})} \tag{7}$$

□

Note that [2,12] propose a better linearization of this convex constraint in a more general context. As a natural complement to the previous proposition, *Proposition* 2 defines a linear process to check whether the two points $u, v \in \mathbb{R}^2$ are sufficiently separated, according to the separation distance d which is a non linear constraint. So this discretization approach also allows to consider minimum separation distance, which is a non convex constraint.

Proposition 2 *Let once again $u, v \in \mathbb{R}^2$ and $d \in \mathbb{R}^+$. Then, the following implication holds*

$$[\ \exists i \in \mathcal{U}, \ \langle u-v \mid U_i \rangle \geq d \ ] \Longrightarrow ||u-v|| \geq d \tag{8}$$

Proof It is a direct consequence of the Cauchy-Schwarz inequality for the canonical inner product of $\mathbb{R}^2$. Let i be the direction such that $\langle u-v \mid U_i \rangle \geq d$, then:

$$\begin{aligned} ||u-v|| &= ||u-v|| \cdot ||U_i|| \quad (\text{since } ||U_i|| = 1) && (9)\\ &\geq |\langle u-v \mid U_i \rangle| && (10)\\ &\geq d && (11) \end{aligned}$$

□

On a practical point of view, when we need to make sure that two points are sufficiently separated, it means that we only need to find, among the $n_{\text{directions}}$ discretized directions, one direction for which this inner product is sufficiently high.

2.2 Quality of the linear approximation

In the case of *Proposition* 1 (the same analysis could be conducted for *Proposition* 2), say we are trying to check whether the distance $d_{uv} \in \mathbb{R}^+$ between two points $u, v \in \mathbb{R}^2$ is lower than $\Delta \in \mathbb{R}^+$. Relying on our previous results, if all the inner products are less or equal to Δ as dictated by *Proposition* 1, we will consider here that $d_{uv} \leq \Delta$.

Though, note that the guarantee resulting from all the inner product inequalities is that the distance between the two points is lower than Δ_{lim} with

$$\Delta_{\text{lim}} = \frac{\Delta}{\cos(\theta_{\max})} \tag{12}$$

This means that the two points could be actually at a distance comprised between Δ and Δ_{lim}, and still be considered as closer than Δ according to the process of *Proposition* 1. This is exactly what is represented in Fig. 1(b): $\mathcal{D}$ is a disk of radius Δ centered on a certain $v \in \mathbb{R}^2$, and $\mathcal{P}$ is the set of points verifying all the inner product inequalities with respect to the point v, i.e. $\mathcal{P} = \{u \in \mathbb{R}^2 \ / \ \forall i \in \mathcal{U}, \langle u - v \mid U_i \rangle \leq \Delta\}$. Therefore, $\mathcal{P} \backslash \mathcal{D}$ is what we could call the exterior approximation set, that is the set of points that are considered at a distance from v less than Δ although they are not. Note that there is another way of exploiting *Proposition* 1 by comparing all the inner products to $\cos(\theta_{\max})\Delta$ instead of directly Δ, then when all the inequalities are true, we have now the guarantee that the distance between the two analyzed points is less or equal to Δ. However, in that case, it is possible to find situations where the distance between the two points is comprised between $\cos(\theta_{\max})\Delta$ and Δ and where one of the inner products has a value greater than $\cos(\theta_{\max})\Delta$, leading to an impossibility to conclude that the two points are closer than Δ with the process of *Proposition* 1. This defines the interior approximation set $\mathcal{D} \backslash \mathcal{P}'$ with $\mathcal{P}' = \{u \in \mathbb{R}^2 \ / \ \forall i \in \mathcal{U}, \langle u - v \mid U_i \rangle \leq \cos(\theta_{\max})\Delta\}$, also represented in Fig. 1(b). In the end, we have to chose between two undesirable consequences of our linear approximation: accepting incorrect close points, or not detecting correct close points. Concerning these two effects, note that the two right-hand sides analyzed here ($\cos(\theta_{\max})\Delta$ and Δ that helped define $\mathcal{P}'$ and $\mathcal{P}$ respectively) correspond to extreme situations. Depending on the application considered, one could try to find a convenient trade-off between the two detrimental effects by chosing a right-hand side $\alpha \in [\cos(\theta_{\max})\Delta, \Delta]$. Concerning the amplitude of the error caused by the linear approximation, it is directly linked to the number of directions $n_{\text{directions}}$: the error tends relatively fast towards 0 when $n_{\text{directions}}$ increases. One way to quantify this convergence is to compare the area of $\mathcal{D}, \mathcal{P}$ and $\mathcal{P}'$ with a varying number of directions, as done in Fig. 2.

2.3 Extension of these principles to $\mathbb{R}^3$ and higher dimensions

The method proposed in section 2.1 for the linearization of euclidean norm constraints is valid in dimension 2. In the following, we argue about the possibility to consider dimension 3.

Another way to interprete this choice we made to rely on the n^{th} roots of unity in $\mathbb{R}^2$ to discretize the Euclidean plane directions is to observe that they are a solution to the following problem: what subset of size $n_{\text{directions}}$ of the $\mathbb{R}^2$ unit circle minimizes the maximum angular distance between a point of the unit circle and its angularly closest point among the selected $n_{\text{directions}}$ points ? Mathematically, this problem can

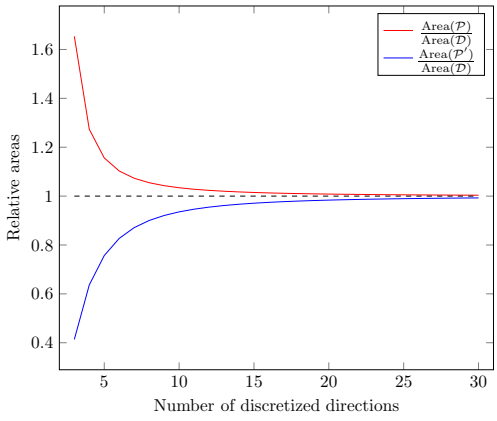

(a)

$n_{\text{directions}}$	$\frac{\text{Area}(\mathcal{P})}{\text{Area}(\mathcal{D})}$	$\frac{\text{Area}(\mathcal{P}')}{\text{Area}(\mathcal{D})}$
4	1.273	0.637
8	1.055	0.900
12	1.023	0.955
16	1.013	0.974
20	1.008	0.984
24	1.006	0.989
28	1.004	0.992

(b)

Fig. 2 (a) Evolution of the area of the approximating polygons $\mathcal{P}$ and $\mathcal{P}'$ with respect to the area of the disk $\mathcal{D}$ (b) Examples of values appearing in the curves

be expressed as follows

$$\min_{\substack{\mathcal{A}\subset\{v\in\mathbb{R}^2 \mid ||v||=1\} \\ \text{s.t. } \text{card}(\mathcal{A})=n_{\text{directions}}}} \mathcal{J}(\mathcal{A}) = \max_{\substack{u\in\mathbb{R}^2 \\ \text{s.t. } ||u||=1}} \min_{u'\in\mathcal{A}} (u, u') \tag{13}$$

and it indeed admits the uniform distribution defined by the n^{th} roots of unity ($\mathcal{A}=\mathcal{U}$) as an optimal solution of optimal value $\mathcal{J}(\mathcal{U}) = \theta_{\max}$ (the entire set of optimal solutions can be obtained by rotating the n^{th} roots of unity of an angle $\alpha \in \left[0, \frac{2\pi}{n_{\text{directions}}}\right)$, each value of α leading to a distinct solution).

While it is trivial in $\mathbb{R}^2$ to discretize uniformly the directions of the plane for a certain number of aimed directions $n_{\text{directions}}$, it is far from obvious to find a predetermined number of uniformly distributed points at the surface of the unit sphere in $\mathbb{R}^3$. For some values of $n_{\text{directions}}$, it can even be proven that there is no solution of exactly uniform distributions of the points on the sphere. As a result, this very simple problem motivated a dedicated wave of research and therefore offers a rich literature on the different methods developed to solve it: [21], [24], [13], [9]. For our linearization process, it means that we have to extend our principles to non-uniform discretized directions in $\mathbb{R}^3$. One way to do so is to solve at best the problem defined previously in $\mathbb{R}^3$:

$$\min_{\substack{\mathcal{A}\subset\{v\in\mathbb{R}^3 \mid ||v||=1\} \\ \text{s.t. } \text{card}(\mathcal{A})=n_{\text{directions}}}} \mathcal{J}(\mathcal{A}) = \max_{\substack{u\in\mathbb{R}^3 \\ \text{s.t. } ||u||=1}} \min_{u'\in\mathcal{A}} (u, u') \tag{14}$$

In some of the aforementioned literature, this problem is exactly the one tackled, but there are articles that also address close variants of the problem with other criteria inspired by physical phenomena, such as electrostatic equilibrium for instance. From the point of view of our application, solving this optimization problem can be

interpreted as finding the most isotropic treatment of all the $\mathbb{R}^3$ directions before approximating linearly the Euclidean distances. Let therefore $\mathcal{U}$ be an optimal (or sub-optimal) solution of (14), then *Proposition* 1 and *Proposition* 2 become valid in $\mathbb{R}^3$ simply by using $\mathcal{U}$ as the set of discretized directions and by setting $\theta_{\max} = \mathcal{J}(\mathcal{U})$. Since the application that motivated this work (beam layout optimization, detailed further in the article) is set in the Euclidean plane, we did not perform at this point any analysis for $\mathbb{R}^3$ similar to the one presented in the previous paragraph for $\mathbb{R}^2$ where the evolution of the approximation error with the number of discretized direction has been properly quantified. To do so, one would simply have to implement a solution for solving (14) for each number of directions $n_{\text{directions}}$ tested.

Finally, note that several articles tackle the question of sampling uniformly from n-dimensional spheres (for instance [8] and [20]), allowing us to further extend our principles to dimensions even higher than $\mathbb{R}^3$ by applying the exact same reasoning.

3 Relation with known approximations of the Euclidean distance

Mukherjee [19] presents approximations of the Euclidean norm based on linear combinations of other norms. He proposes a combination of the L_∞ and L_1 norms and also a combination of the euclidean chamfering weighted distance in n-D (CWD_{eu}) and the inverse square root weighted t-cost distance in n-D (WtD_{isr}). We give below the expression of these different norms for a 2-D vector $u = \begin{pmatrix} u_x \\ u_y \end{pmatrix}$.

$$d_{L_\infty}(u) = \max(|u_x|, |u_y|) \tag{15}$$

$$d_{L_1}(u) = |u_x| + |u_y| \tag{16}$$

$$d_{WtD_{isr}}(u) = \max\left(\max(|u_x|, |u_y|), \frac{1}{\sqrt{2}}(|u_x| + |u_y|)\right) \tag{17}$$

$$\begin{aligned} d_{CWD_{eu}}(u) &= \max(|u_x|, |u_y|) + (\sqrt{2}-1)\min(|u_x|, |u_y|) \\ &= (2-\sqrt{2})\max(|u_x|, |u_y|) + (\sqrt{2}-1)\,((|u_x| + |u_y|)) \end{aligned} \tag{18}$$

The latter expression is obtained by using the relation $\min(|u_x|, |u_y|) = |u_x| + |u_y| - \max(|u_x|, |u_y|)$. Norms L_∞ and WtD_{isr} give under-estimations of the Euclidean norm, while norms L_1 and CWD_{eu} provide over-estimations of the Euclidean norm. We use the second expression of norm CWD_{eu} since it allows an easier linearization.

Now, let $U^{n,\alpha}$ the 2×n matrix such that each vector column $(U_i^{n,\alpha})_{i=1,\cdots,n}$ is the direction obtained by expression (1) with $n_{\text{directions}} = n$ and then rotated by angle α. We consider in particular the following matrices:

$$U^{4,0} = \begin{pmatrix} 1 & 0 & -1 & 0 \\ 0 & 1 & 0 & -1 \end{pmatrix} \quad U^{4,\frac{\pi}{4}} = \begin{pmatrix} \cos(\frac{\pi}{4}) & -\cos(\frac{\pi}{4}) & -\cos(\frac{\pi}{4}) & \cos(\frac{\pi}{4}) \\ \cos(\frac{\pi}{4}) & \cos(\frac{\pi}{4}) & -\cos(\frac{\pi}{4}) & -\cos(\frac{\pi}{4}) \end{pmatrix}$$

$$U^{8,0} = \begin{pmatrix} 1 & \cos(\frac{\pi}{4}) & 0 & -\cos(\frac{\pi}{4}) & -1 & -\cos(\frac{\pi}{4}) & 0 & \cos(\frac{\pi}{4}) \\ 0 & \cos(\frac{\pi}{4}) & 1 & \cos(\frac{\pi}{4}) & 0 & -\cos(\frac{\pi}{4}) & -1 & -\cos(\frac{\pi}{4}) \end{pmatrix}$$

$$U^{8,\frac{\pi}{8}} = \begin{pmatrix} \cos(\frac{\pi}{8}) & \sin(\frac{\pi}{8}) & -\sin(\frac{\pi}{8}) & -\cos(\frac{\pi}{8}) & -\cos(\frac{\pi}{8}) & -\sin(\frac{\pi}{8}) & \sin(\frac{\pi}{8}) & \cos(\frac{\pi}{8}) \\ \sin(\frac{\pi}{8}) & \cos(\frac{\pi}{8}) & \cos(\frac{\pi}{8}) & \sin(\frac{\pi}{8}) & -\sin(\frac{\pi}{8}) & -\cos(\frac{\pi}{8}) & -\cos(\frac{\pi}{8}) & -\sin(\frac{\pi}{8}) \end{pmatrix}$$

Let $\mathcal{P}_n^{\alpha} = \{u \in \mathbb{R}^2 \ / \ \forall i \in \{1,\cdots,n\}, \langle u \mid U_i^{n,\alpha} \rangle \leq \Delta\}$ the set of points that lie at a distance of no more than Δ from the origin according to the outer approximation of the Euclidean distance via discretization $U^{n,\alpha}$ and let $\mathcal{P}'^{\alpha}_n = \{u \in \mathbb{R}^2 \ / \ \forall i \in \{1,\cdots,n\}, \langle u \mid U_i^{n,\alpha} \rangle \leq \cos(\frac{\pi}{n})\Delta\}$ the set of points that lie at a distance of no more than Δ from the origin according to the inner approximation of the Euclidean distance via discretization $U^{n,\alpha}$.

Proposition 3 *Let $\delta \in \mathbb{R}^+$. Consider the set of points*

$$\mathcal{P}_{L_\infty} = \{u \in \mathbb{R}^2 \ / \ d_{L_\infty}(u) \leq \Delta\} \quad \mathcal{P}_{L_1} = \{u \in \mathbb{R}^2 \ / \ d_{L_1}(u) \leq \Delta\}$$

$$\mathcal{P}_{WtD_{isr}} = \{u \in \mathbb{R}^2 \ / \ d_{WtD_{isr}}(u) \leq \Delta\} \quad \mathcal{P}_{CWD_{eu}} = \{u \in \mathbb{R}^2 \ / \ d_{CWD_{eu}}(u) \leq \Delta\}$$

We have the following:

$$(i)\, \mathcal{P}_{L_\infty} = \mathcal{P}_4^0, (ii)\, \mathcal{P}_{L_1} = \mathcal{P}'^{\frac{\pi}{4}}_4, (iii)\, \mathcal{P}_{WtD_{isr}} = \mathcal{P}_8^0 \text{ and } (v)\, \mathcal{P}_{CWD_{eu}} = \mathcal{P}'^{\frac{\pi}{8}}_8$$

Proof

$$(i)\ \max(|u_x|,|u_y|) \leq \Delta \Leftrightarrow \begin{cases} u_x \leq \Delta \\ u_y \leq \Delta \\ -u_x \leq \Delta \\ -u_y \leq \Delta \end{cases} \Leftrightarrow \left\langle u \mid U_i^{4,0} \right\rangle \leq \Delta \quad \forall i = 1,\cdots,4$$

$$(ii)\ |u_x| + |u_y| \leq \Delta \Leftrightarrow \begin{cases} u_x + u_y \leq \Delta \\ -u_x + u_y \leq \Delta \\ -u_x - u_y \leq \Delta \\ u_x - u_y \leq \Delta \end{cases} \Leftrightarrow \begin{cases} \cos(\frac{\pi}{4})u_x + \cos(\frac{\pi}{4})u_y \leq \cos(\frac{\pi}{4})\Delta \\ -\cos(\frac{\pi}{4})u_x + \cos(\frac{\pi}{4})u_y \leq \cos(\frac{\pi}{4})\Delta \\ -\cos(\frac{\pi}{4})u_x - \cos(\frac{\pi}{4})u_y \leq \cos(\frac{\pi}{4})\Delta \\ \cos(\frac{\pi}{4})u_x - \cos(\frac{\pi}{4})u_y \leq \cos(\frac{\pi}{4})\Delta \end{cases}$$

$$\Leftrightarrow \left\langle u \mid U_i^{4,\frac{\pi}{4}} \right\rangle \leq \cos(\tfrac{\pi}{4})\Delta \quad \forall i = 1,\cdots,4$$

$$(iii)\ \max\left(\max(|u_x|,|u_y|), \tfrac{1}{\sqrt{2}}(|u_x| + |u_y|)\right) \leq \Delta \Leftrightarrow \begin{cases} u_x \leq \Delta \\ -u_x \leq \Delta \\ u_y \leq \Delta \\ -u_y \leq \Delta \\ \frac{1}{\sqrt{2}}u_x + \frac{1}{\sqrt{2}}u_y \leq \Delta \\ -\frac{1}{\sqrt{2}}u_x + \frac{1}{\sqrt{2}}u_y \leq \Delta \\ \frac{1}{\sqrt{2}}u_x - \frac{1}{\sqrt{2}}u_y \leq \Delta \\ \frac{1}{\sqrt{2}}u_x - \frac{1}{\sqrt{2}}u_y \leq \Delta \end{cases}$$

$$\Leftrightarrow \left\langle u \mid U_i^{8,0} \right\rangle \leq \Delta \quad \forall i = 1,\cdots,8$$

since $\cos(\frac{\pi}{4}) = \frac{1}{\sqrt{2}}$.

(iv) $(2-\sqrt{2})\max(|u_x|,|u_y|)+(\sqrt{2}-1)\ ((|u_x|+|u_y|)) \leq \Delta$

$$\Leftrightarrow \begin{cases} |u_x|+(\sqrt{2}-1)|u_y| \leq \Delta \\ (\sqrt{2}-1)|u_x|+|u_y| \leq \Delta \end{cases}$$

since $\sqrt{2} = 2\cos(\frac{\pi}{4})$ we have:

$$\Leftrightarrow \begin{cases} \cos(\frac{\pi}{8})|u_x|+\cos(\frac{\pi}{8})(2\cos(\frac{\pi}{4})-1)|u_y| \leq \cos(\frac{\pi}{8})\Delta \\ \cos(\frac{\pi}{8})(2\cos(\frac{\pi}{4})-1)|u_x|+\cos(\frac{\pi}{8})|u_y| \leq \cos(\frac{\pi}{8})\Delta \end{cases}$$

using $2\cos(a)\cos(b) = \cos(a-b)+cos(a+b)$ and $\cos(\frac{3\pi}{8}) = \sin(\frac{\pi}{8})$ we obtain:

$$\Leftrightarrow \begin{cases} \cos(\frac{\pi}{8})|u_x|+\sin(\frac{\pi}{8})|u_y| \leq \cos(\frac{\pi}{8})\Delta \\ \sin(\frac{\pi}{8})|u_x|+\cos(\frac{\pi}{8})|u_y| \leq \cos(\frac{\pi}{8})\Delta \end{cases}$$

$$\Leftrightarrow \left\langle u \mid U_i^{8,\frac{\pi}{8}} \right\rangle \leq \cos(\tfrac{\pi}{8})\Delta \quad \forall i = 1,\cdots,8$$

□

It follows that the proposed scheme based on uniform discretization of the plane directions allows to include in mixed-integer linear programs the previously proposed norms L_1, $L\infty$, WtD_{isr} and CWD_{eu} as well as their linear and convex combinations proposed in [19]. As these norms correspond to the particular cases $n_{\text{directions}} = 4$ and $n_{\text{directions}} = 8$, this framework allows to obtain their generalization to higher discretization levels, improving as needed w.r.t the acceptable CPU time increase the approximation quality. Note that in our experiments, the linear combination of under- and over-estimated norms would lead to significant violations of the constraints. Hence for maximal distance constraints, we use a over-estimate of the Euclidean distance while for the minimal distance constraints, we use an under-estimate of the Euclidean distance.

4 A simple case with convex distance constraints: the continuous k-center problem

To illustrate the applicability of the proposed linearization process, this section introduces how it could be used to solve a well-known operations research problem that mixes continuous and discrete aspects: the continuous k-center problem. It consists in defining the position of $K \geq 1$ centers that are used to cover $N \geq 1$ cities of known positions $\mathcal{C}_c = (X_c, Y_c) \in \mathbb{R}^2$ ($c \in \{1,\cdots,N\}$) in order to provide a certain service: these centers can be fire stations, hospitals, police stations, warehouses... The goal is to place the centers and to allocate the cities to the centers in such a way as to minimize the maximum time needed to provide service to a city. To produce such solutions, most of the literature on the continuous k-center problem proposes to minimize the maximum Euclidean distance between a center and its allocated stations,

but other norms can be used, as it is done in [23] with l_1 and l_∞ norms for instance. Here, we naturally consider the Euclidean norm in order to apply the linearization principles presented in the previous section. We use continuous variables for the position of the K centers ($(x_k, y_k) \in \mathbb{R}^2,\ k \in \{1,\cdots,K\}$), that are allowed to vary in a certain bounding box $\mathcal{B} = [\mathcal{X}_{\min}, \mathcal{X}_{\max}] \times [\mathcal{Y}_{\min}, \mathcal{Y}_{\max}] \subset \mathbb{R}^2$, and boolean variables to materialize the allocation of the cities to the centers ($\alpha_{c,k} \in \{0,1\}$). Finally, $\lambda \in \mathbb{R}^+$ is the continuous variable that will represent the maximum distance of a city to its center (that is to be minimized).

$$\text{Minimize} \quad \lambda \tag{19}$$

under the following constraints

$$\forall k \in \{1,\cdots,K\}, \quad x_k \geq \mathcal{X}_{\min} \tag{20}$$

$$\forall k \in \{1,\cdots,K\}, \quad x_k \leq \mathcal{X}_{\max} \tag{21}$$

$$\forall k \in \{1,\cdots,K\}, \quad y_k \geq \mathcal{Y}_{\min} \tag{22}$$

$$\forall k \in \{1,\cdots,K\}, \quad y_k \leq \mathcal{Y}_{\max} \tag{23}$$

$$\forall c \in \{1,\cdots,N\}, \quad \sum_{k \in \{1,\cdots,K\}} \alpha_{c,k} = 1 \tag{24}$$

$$\forall c \in \{1,\cdots,N\}, \forall k \in \{1,\cdots,K\},$$

$$\alpha_{c,k} \in \{0,1\} \tag{25}$$

$$\sqrt{(x_k - X_c)^2 + (y_k - Y_c)^2} \leq \lambda + M_c(1 - \alpha_{c,k}) \tag{26}$$

The MINLP described by equations (19)-(26) corresponds to the minimization of the maximum distance between a center and its associated cities. Equations (20), (21), (22), (23) define the boundaries of the center positions. The constraints (24) force each city to be allocated to one and only center. Finally, the constraints (26) allows to lower-bound the continuous distance variable λ by all the center-city distances of all active center-city couples. This constraint is a non linear but convex distance proximity constraint. Furthermore, it involves a big M constraint where M_c can be formulated as the greatest distance between a city and a position in the bounding box. So we can consider $M_c = \max_{Z \in \mathcal{B}} \|Z - C_c\|$. By means of *Proposition* 1, we can reformulate (26) by

$\forall c \in \{1,\cdots,N\}, \forall k \in \{1,\cdots,K\}, \forall u \in \{1,\cdots,n_{\text{directions}}\}$,

$$\cos(\theta_{\max})\lambda \geq \begin{pmatrix} x_k - X_c \\ y_k - Y_c \end{pmatrix} \cdot \begin{pmatrix} U_{u,x} \\ U_{u,y} \end{pmatrix} - M_c(1 - \alpha_{c,k}) \tag{27}$$

Note that in equations (31), *Proposition* 1 is used with a "conservative" approach: the unit disk is approximated by $\mathcal{P}'$ in order to over-estimate the minimized maximum distance, instead of under-estimating it as it would have been the case with an

approximation of the disk by $\mathcal{P}$. Fig. 3 provides examples of solutions generated by this MILP respectively for ($N = 59$, $K = 9$, $n_{\text{directions}} = 12$) and ($N = 144$, $K = 30$, $n_{\text{directions}} = 12$). Note that in this problem, there are no strict proximity constraints,

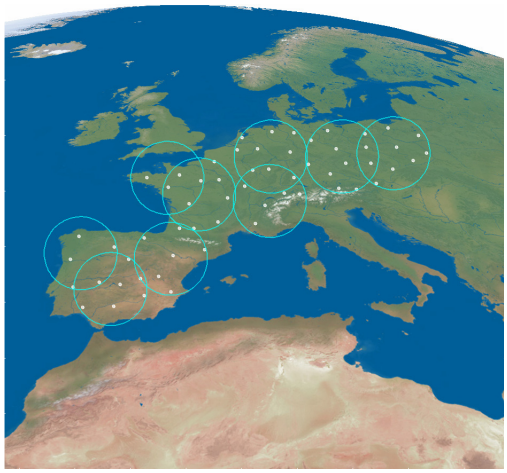

(a)

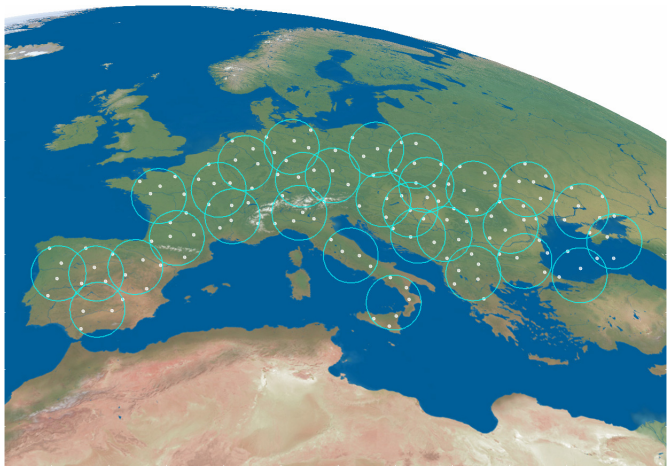

(b)

Fig. 3 (a) k-center solution example for $N = 59$, $K = 9$, $n_{\text{directions}} = 12$(b) k-center solution example for $N = 144$, $K = 30$, $n_{\text{directions}} = 12$

nor separation constraints, but simply a notion of maximum distance to be minimized. This allows to have a wide range of different strategies based on branch-and-bound procedures (see [10] for instance) or on metaheuristics ([22]) to produce optimal solutions for very large instances that we could not solve with the MILP model above. However, this example seemed simple enough to illustrate how easily our linearization process allows to reach a direct algorithmic solution that relies on all the powerful

solving principles inherent to Mixed Integer Linear Programming. Most importantly, such models are adaptable to variants of the problem that are characterized by extra sets of constraints and variables.

As mentioned in Section 2, the authors of [16] propose linearization and discretization techniques for a special sphere covering problem occuring in a gamma ray machine radiosurgery application. Their technique is based on the linearization of the squared distance. Below we apply this technique to the $k-center$ problem so as to make an experimental comparison with our approach for different discretization levels. The approach considered the squared distance $(x_k - X_c)^2 + (y_k - Y_c)^2 = x_k^2 + y_k^2 - 2x_kX_c - 2y_kY_c + X_c^2 + Y_c^2$, where the only non linear variable terms are x_k^2 and y_k^2. The linearization is based on a discretization parameter D and on points

$$\bar{x}_d = \mathcal{X}_{\min} + (d-1)\frac{\mathcal{X}_{\max} - \mathcal{X}_{\min}}{D} \quad d = 1,\ldots,D$$

$$\bar{y}_d = \mathcal{Y}_{\min} + (d-1)\frac{\mathcal{Y}_{\max} - \mathcal{Y}_{\min}}{D} \quad d = 1,\ldots,D$$

Then the piecewise linear function defined by segments $(\bar{x}_d, \bar{x}_d^2)(\bar{x}_{d+1}, \bar{x}_{d+1}^2)$ for $d = 1,\ldots,D-1$ defines an inner approximation of x^2 of any $x \in [\mathcal{X}_{\min}, \mathcal{X}_{\max}]$ and the one defined by segments $(\bar{y}_d, \bar{y}_d^2)(\bar{y}_{d+1}, \bar{y}_{d+1}^2)$ for $d = 1,\ldots,D-1$ defines an inner approximation of y^2 of any $y \in [\mathcal{Y}_{\min}, \mathcal{Y}_{\max}]$. It follows that constraints (26) is implied by the following constraints, introducing continuous variables $\hat{x}_k$ and $\hat{y}_k$ as upper bounds of x_k^2 and y_k^2, and variable $\Lambda = \lambda^2$.

$\forall c \in \{1,\cdots,N\}, \forall k \in \{1,\cdots,K\},$

$$\hat{x}_k + \hat{y}_k - 2x_kX_c - 2y_kY_c + X_c^2 + Y_c^2 \leq \Lambda + M_c^2(1 - \alpha_{c,k}) \tag{28}$$

$\forall k \in \{1,\cdots,K\}, \forall d \in \{1,\cdots,D-1\}$

$$\hat{x}_k \geq (\bar{x}_{d+1} + \bar{x}_d)x_k - \bar{x}_{d+1}\bar{x}_d \tag{29}$$

$$\hat{y}_k \geq (\bar{y}_{d+1} + \bar{y}_d)y_k - \bar{y}_{d+1}\bar{y}_d \tag{30}$$

Constraints (28) bounds the squared maximum distance Λ, whereas constraints (29) and (29) enforce $\hat{x}_k \geq x_k^2$ and $\hat{y}_k \geq y_k^2$, by convexity. Then the approach of [16] applied to the $k-$center problem consists in solving the following MILP:

Minimize Λ
under constraints (20–25), (28–30).

As, on one hand, no theoretical bound on the approximation error is provided in [16] and, on the other hand, no inclusion of the linear combinations of norms in optimization models were tested in [19], we opt for an experimental comparison. We consider a set of 60 instances of the $k-$center problem including 10 instances of each of the following families, from small to medium size: $N = 50/K = 5$, $N = 70/K = 7$, $N = 80, K = 8$, $N = 100/K = 10$, $N = 120/K = 12$, $N = 130/K = 13$. The N points

have been randomly selected from a set of 157 points issued from the multibeam satellite design application (see next section).

We compare our linearization scheme with $n_{\text{directions}} \in \{4,8,12,14,16,20\}$ (denoted DIR), the linearization proposed by Liberti et al. [16] (denoted L) with $D \in \{10,20,30,40\}$. We also include in the experiments two linear combinations of norms proposed by Mukherjee [19]: the linear combination of L_1 with weight $a = 0.39$ and L_∞ with weight $b = 0.55$ and the linear combination of CWD_{eu} with weight $a = 0.47$ and WtD_{isr} with weight $b = 0.51$. These weights have been empirically determined as good for minimizing the maximal relative error in [19]. For each of these two linear combinations, we compare two linearizations. The first ones, denoted NL1LI for the combination of L_1 and L_∞ and NWC for the second combination, are based on the "natural" linearization of the max and absolute value operators, which here does not require any adjunction of binary variables. We refer to proof of Proposition 3 for the transformation of an upper bounding constraint on these operators in a conjunction of linear contraints. The to other linearizations, denoted DL1LI and DWC, respectively, are based on the equivalent representations of the norms by the discretization of the directions of the planes established by Proposition 3. Hence we combine the over-estimating distance with directions $U^{n,0}$ and the underestimating distance with directions $U^{n,\frac{\pi}{n}}$ with $n \in \{4,8\}$. To that purpose, proximity constraints have to be checked for each pair of directions $U_u^{n,0}$ and $U_v^{n,\frac{\pi}{n}}$ for $u,v \in \{1,\cdots,n_{\text{directions}}\}$. Constraints constraints (31) are thus replaced by:

$$\forall c \in \{1,\cdots,N\}, \forall k \in \{1,\cdots,K\}, \forall u,v \in \{1,\cdots,n\},$$

$$\lambda \geq \frac{a}{\cos(\theta_{\max})} \begin{pmatrix} x_k - X_c \\ y_k - Y_c \end{pmatrix} \cdot \begin{pmatrix} U_{u,x}^{n,\frac{\pi}{n}} \\ U_{u,y}^{n,\frac{\pi}{n}} \end{pmatrix} + b \begin{pmatrix} x_k - X_c \\ y_k - Y_c \end{pmatrix} \cdot \begin{pmatrix} U_{v,x}^{n,0} \\ U_{v,y}^{n,0} \end{pmatrix} - M_c(1 - \alpha_{c,k}) \quad (31)$$

All formulations are solved on an 8-core Intel i7-4770 processor clocked at 3.40GHz with 8 GB RAM under Linux Ubuntu 4.4.0-135-generic by the parallel CPLEX 12.6 MILP solver with the default parameters. The results displayed in Tables 1 and 2 provide the average maximum distance, the number of verified optimal solutions and the average CPU time obtained by each approach on each family of instances for a maximum CPU time of 500s. The displayed objective values are the actual distances computed a posteriori on the output solutions. The best solutions are underlined and bolded.

The linearization method of [16] L40 obtains the best results for instances from $N = 50$ to $N = 80$ but the DIR20 approach is close. On the $N = 80$ instances, the linear combination of the CWD_{eu} and WtD_{isr} norms obtain the best results. On the large instances $N = 120$ and $N = 130$, the DIR linearization scheme obtains (by far) the best results for 12 and 16 directions. This justifies to select the DIR scheme for the more complex problem issued from the industrial context presented in section 5, for which at most 100 stations have to be covered. For the DIR and L methods, the increase on the solution quality brought by increasing the discretization level appears clearly for for $N = 50,70,80$ instances. For the large instaces this motonone behavior still holds for the L linearization while for the DIR scheme, the assigned CPU time is sometimes not sufficient for the larger discretization levels. For modest CPU time allowance

	$N = 50$			$N = 70$			$N = 80$		
DIR4	1031.5	10	0.3	833.2	10	1.0	772.3	8	203.4
DIR8	842.7	10	0.5	688.1	10	27.2	640.2	1	489.3
DIR12	822.2	10	0.8	662.4	10	127.4	624.3	0	500.0
DIR14	819.5	10	1.0	659.8	8	191.7	618.6	0	500.7
DIR16	815.9	10	1.2	658.2	8	195.1	616.5	0	500.1
DIR20	812.7	10	1.4	655.8	9	192.1	612.2	0	500.1
L10	819.0	10	1.6	675.2	10	17.9	632.6	10	63.7
L20	808.7	10	1.5	655.7	10	31.4	612.9	10	111.8
L30	806.7	10	1.6	652.7	10	44.8	610.6	9	167.7
L40	**806.3**	10	1.7	**652.3**	10	40.2	**610.4**	7	189.8
NL1LI	844.4	10	9.4	683.2	1	483.9	641.5	0	500.0
DL1LI	847.8	10	12.8	686.7	0	500.0	644.3	0	500.1
NWC	814.6	10	19.6	658.9	1	461.1	614.8	0	500.1
DWC	814.4	10	5.8	658.8	10	37.3	619.4	9	175.5

Table 1 Comparison of linearizations with a 500s CPU time limit for $N = 50, 70, 80$

	$N = 100$			$N = 120$			$N = 130$		
DIR4	703.9	0	500.1	618.4	0	500.2	598.9	0	500.4
DIR8	583.0	0	500.0	532.4	0	500.1	507.6	0	500.1
DIR12	562.6	0	500.0	**515.6**	0	500.1	502.6	0	500.1
DIR14	560.5	0	500.1	521.6	0	500.1	513.8	0	500.1
DIR16	557.7	0	500.1	518.7	0	500.1	**500.8**	0	500.1
DIR20	566.9	0	500.1	535.1	0	501.0	571.6	0	500.4
L10	581.6	3	464.8	610.9	0	500.0	664.1	0	500.1
L20	588.7	2	462.9	678.8	0	500.1	666.9	0	500.0
L30	593.8	0	500.1	685.4	0	500.1	716.4	0	500.0
L40	601.3	3	465.9	626.4	0	500.0	637.7	0	500.0
NL1LI	569.2	0	500.1	562.1	0	500.1	561.7	0	500.1
DL1LI	678.6	0	500.1	762.9	0	500.1	801.0	0	500.1
NWC	**553.7**	0	500.1	525.3	0	500.1	526.8	0	500.1
DWC	661.5	0	500.1	776.5	0	500.1	768.8	0	500.2

Table 2 Comparisons of linearizations with a 500s CPU time limit for $N = 100, 120, 130$

the DIR8 and DIR12 linearizations are very competitive. Remarkably, the natural linearizations of the linear combinations NWC obtain consistently results close to the best solution for all instance sets. However, except for $N = 80$, they are always outperformed by at lest one DIR linearization. The linear combination NL1LI is less competitive and most often ranked far behinf DIR8. Finally, it appears by comparing rows that the linearizations of the linear combinations of norm following the plane direction scheme (DL1LI and DWC) are less efficient for large instances than the adhoc linearization NL1LI and NWC, respectively. Note that the different objective values in the case that all instances are solved to optimality for example for $N = 50$, DL1LI and NL1LI is explained by the fact that, although both formulations have the same optimal value, the centers are not located at the same points and the true L2 distances can vary.

To illustrate the approximation quality of the different linearizations, we provide for each linearization the relative deviation from the estimated maximum distance (MILP objective value) and the actual maximum distance. More precisely is $\bar{\lambda}$ is the actual maximum distance of the solution (computed a posteriori) and λ^* is the MILP

	Average deviation	Max deviation	Min deviation
DIR4	-0.46%	0.00%	-6.98%
DIR8	-0.12%	0.00%	-1.10%
DIR12	-0.03%	0.00%	-0.65%
DIR14	-0.07%	0.00%	-0.67%
DIR16	-0.04%	0.00%	-0.70%
DIR20	-0.03%	0.00%	-0.51%
L10	-1.40%	-0.95%	-1.85%
L20	-0.22%	-0.21%	-0.22%
L30	-0.12%	-0.05%	-0.19%
L40	-0.02%	-0.02%	-0.02%
NL1LI	5.63%	6.00%	0.54%
DL1LI	5.77%	6,00%	3,63%
NWC	1.92%	2,05%	0.93%
DWC	1.89%	2.01%	1.01%

Table 3 Average, Maximum and Minimum deviation from the actual Euclidean distance

objective function value. The deviation is $\frac{\bar{\lambda}-\lambda^*}{\lambda*}$. Table 3 gives the average, maximal and minimal deviation obtained by the methods on the 60 instances.

The figures illustrate that the DIR and L linearizations provide over-approximations of the Euclidean distance. The impact of the discretization level on the magnitude of the error appears clearly, with a negligible error from $N_{\text{directions}} \geq 12$ for DIR and from $D \geq 40$ for L. On the opposite, the linear combinations of norms tend to underestimate the maximal distance (although the distance is generally neither an under- nor an over-approximation) with rather high deviations for the L1LI linear combination and better deviations for the WC linear combination, which is consistent with the findings in [19].

5 A more complex application with non convex distance constraints: the beam layout optimization problem in multibeam satellite systems

5.1 Coordinate system used to define the optimization problem

This paragraph describes the coordinate system used to identify the points on the Earth's surface in the context of satellite communications. It is a necessary information to understand the beam layout optimization problem as it is presented in the next paragraph. A well-known reference system in this application (see [4] for instance) is the satellite-centered (x,y,z) coordinate system, presented on Fig. 4(a). The z axis is in the satellite-Earth centre direction, the x axis is perpendicular to the meridian plane of the satellite (defined by the North, the z axis, and the position of the satellite) and is oriented toward the east, and the y axis is perpendicular to the equatorial plane and oriented in such a way as to complete a right-handed coordinate system (i.e. the south for a geostationary satellite). On the figure, S represents the satellite, O the centre of the Earth, P a point on the Earth's surface and $\hat{P}$ its projection on the equatorial plane.

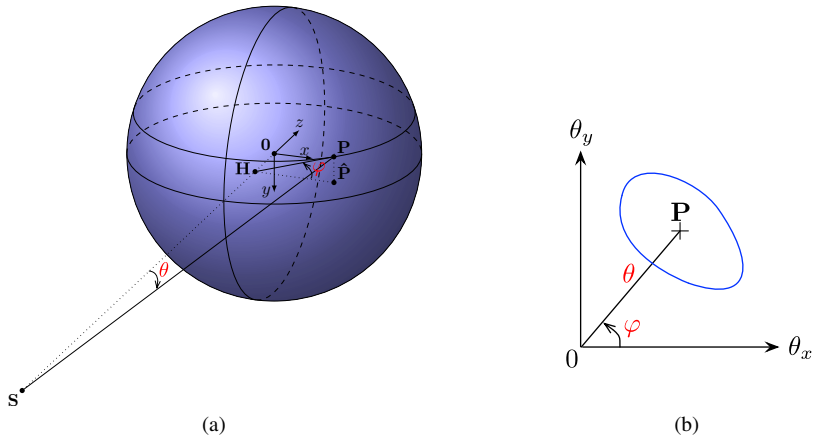

Fig. 4 (a) Satellite-centered coordinate system and true view angles (b) True view representation

Let us denote by $\mathcal{A}$ the set of points on the Earth's surface that are visible from the satellite. Let Θ be the set of possible angles between the $\overrightarrow{z}$ direction and the $\overrightarrow{SP}$ directions when $P \in \mathcal{A}$, and let Φ be the set of possible $(\overrightarrow{H\hat{P}}, \overrightarrow{HP})$ angles when $P \in \mathcal{A}$ with H being its projection on the $\overrightarrow{SO}$ line and $\hat{P}$ being its projection on the equatorial plane. Then, a useful property is that there exists a subset $\mathcal{Z}$ of $\Theta \times \Phi$ and a bijection from $\mathcal{A}$ into $\mathcal{Z}$ that allows us to use the couple of true view angles $(\theta, \varphi) \in \mathcal{Z}$, as they are called, to completely identify any point P in $\mathcal{A}$, as shown in Fig. 4(a). In this figure, there is also an illustration of the notion of angular separation of two points on the surface of the Earth from the point of view of the satellite, which is crucial for the problem we addressed in this paper: there is indeed an example of such an angular separation with θ, which is the angle between the sub-satellite point (on the surface of the Earth) and the point P.

There exists a very convenient representation of these true view angles in the xy plane. To the two true view angles (θ, φ) of a given point P in $\mathcal{A}$, we associate the so called projected true view angles $\theta_x \in \Theta_x$ and $\theta_y \in \Theta_y$ defined as follows:

$$\theta_x = \theta \cos \varphi \tag{32}$$

$$\theta_y = \theta \sin \varphi \tag{33}$$

which bijectively defines Θ_x and Θ_y from $\mathcal{Z}$, as represented in figure (b) of Fig. 4. A well known result on these projected true view angles is that, for any two points P_1 and P_2 in $\mathcal{A}$, the following approximation

$$\left|(\overrightarrow{SP_1}, \overrightarrow{SP_2})\right| \simeq \sqrt{(\theta_{x,P_2} - \theta_{x,P_1})^2 + (\theta_{y,P_2} - \theta_{y,P_1})^2} \tag{34}$$

is perfectly acceptable in the case of geostationary satellites (see [4] for instance for more details on this point). This means that the angular distance from the point of view of the satellite between two points on the surface of the Earth can be computed

with a simple Euclidean norm in the projection space $\Theta_x \times \Theta_y$. For this very reason, these coordinates have been chosen for our study and our models.

5.2 Definition of the problem: variables, constraints and objective

A multibeam satellite is a particular type of telecommunication satellite that provides service to its users thanks to a plurality of relatively narrow beams, a beam being a zone of significant electromagnetic power on the surface of the Earth for a given radiofrequency source. After receiving the signals from a gateway connected to the terrestrial network, the satellite payload converts in frequency, amplifies, and retransmits the input signals in the different beams through the reflector antennas, as depicted in Fig. 5 where we have 13 beams transmitted by 4 reflector antennas (one per color in the figure). In the coordinate system presented in section 5.1, and

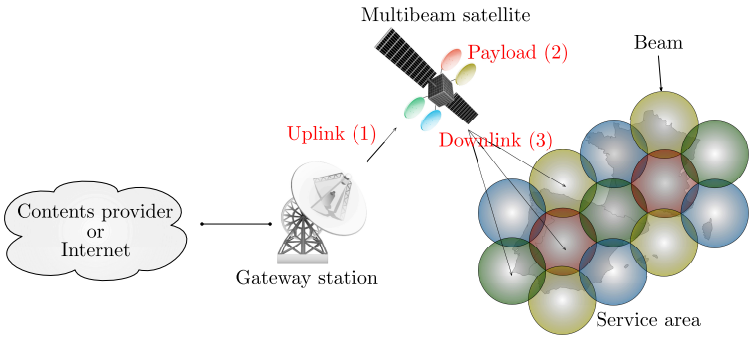

Fig. 5 Standard architecture of a multibeam satellite system

with the antenna technology considered in this work, a beam can be represented as a disk of a certain diameter and with a certain center on the surface of the Earth. The telecommunication mission is defined by a finite set $\mathcal{S} = \{1, \cdots, N_S\}$ of N_S user stations, each station $s \in \mathcal{S}$ being characterized by a traffic demand $T_s \in \mathbb{R}^+$ in Megabits per second and coordinates $S_{\text{coord},s} = (X_{\text{stations},s}, Y_{\text{stations},s}) \in \mathbb{R}^2$. The traffic of a station is considered covered if the station belongs to at least one disk representation of a beam: this condition makes the connection with our work in section 2 on Euclidean proximity constraints. We denote by N_B the number of beams than can be embarked on the satellite, and by $\mathcal{B}$ the set indexing them. When optimizing a beam layout, each beam $b \in \mathcal{B}$ must be assigned a beam center $(x_b, y_b) \in \mathbb{R}^2$ and a diameter in a finite set $\mathcal{W} = \{1, \cdots, N_W\}$ of possibilities: $\{W_1, \cdots, W_{N_W}\} \subset \mathbb{R}^+$. Each beam $b \in \mathcal{B}$ is transmitted by exactly one of the N_R available satellite reflectors, indexed by $\mathcal{R} = \{1, \cdots, N_R\}$. For antenna feasibility reasons detailed in [5], two beams associated to the same reflector must have sufficiently separated beam centers, which makes the link with our work on Euclidean separation constraints in section 2 . The rule adopted in this study is that this separation distance is proportional to the mean

of two beam diameters, according to a proportionality coefficient $\kappa \in \mathbb{R}^+$ (physically realistic values varying in $[\frac{3}{2}, \sqrt{3}]$). Finally, the objective is to maximize the covered traffic.

5.3 NP-hardness of the beam layout optimization

The Circle Covering Problem (CCP) is defined as the following decision problem:

Let $x_1, \cdots, x_n \in \mathbb{R}^2$ be n points of the Euclidean plane and let $p \in \mathbb{N}^*$.
Can we find p unit disks $D_1, \cdots, D_p \subset \mathbb{R}^2$ such that each point is covered by at least one disk ?

In [18], the authors prove that the Circle Covering Problem (CCP) is NP-complete. The beam layout decision problem (BLDP) associated to the beam layout optimization problem defined in the previous paragraph is the following

Let $\zeta \in \mathbb{R}^+$.
Can the aggregate covered traffic $\sum T_s$ be greater than or equal to ζ under the constraints of section 5.2 ?

Proposition 4 *CCP can be reduced polynomially to BLDP. The beam layout optimization problem is therefore NP-hard.*

Proof Let n and p be two positive integers defining an instance I of CCP. We are looking for an instance I' of BLDP polynomially defined from I and such that I true $\Leftrightarrow$ I' true. Let therefore I' be defined as follows: $N_S = n$, $T_s = 1$ for all $s \in \mathcal{S}$, $\zeta = n$, $N_B = p$, $N_R = N_B$, $\kappa = 0$, $N_W = 1$ and $W_1 = 2$. Finally, for all $s \in \mathcal{S}$, the position of the station s in the plane coincides with the s^{th} point of I. Since there is one reflector per beam there is no reflector selection problem. There is no diameter selection constraint neither. Finally, since $\kappa = 0$, there is no separation constraints (the circles can be as close as needed). The problem becomes: can all the N_S stations be covered by N_B beams of radius 1 (no further constraints) ? Thus, the equivalency with I follows. □

5.4 Mixed Integer Linear Programming model

Relying fully on the principles of section 2 a MILP model can be obtained from the following MINLP:

$$\text{Maximize} \sum_{(s,b)\in\mathcal{S}\times\mathcal{B}} T_s\, \alpha_{s,b} \tag{35}$$

under the following constraints

$$\forall s \in \mathcal{S}, \quad \sum_{b\in\mathcal{B}} \alpha_{s,b} \leq 1 \tag{36}$$

$$\forall b \in \mathcal{B}, \quad \sum_{w\in\mathcal{W}} \omega_{b,w} = 1 \tag{37}$$

$$\forall b \in \mathcal{B}, \quad \sum_{r\in\mathcal{R}} \rho_{b,r} = 1 \tag{38}$$

$$\forall s \in \mathcal{S}, \forall b \in \mathcal{B},$$

$$\sqrt{(x_b - X_{\text{stations},s})^2 + (y_b - Y_{\text{stations},s})^2} \leq \sum_{w\in\mathcal{W}} \frac{W_w}{2}\omega_{b,w} + (1-\alpha_{s,b})M_s \tag{39}$$

$$\forall b, b' \in \mathcal{B} \text{ such that } b' > b, \forall r \in \mathcal{R}, \quad \beta_{b,b'} + \rho_{b,r} + \rho_{b',r} \leq 2 \tag{40}$$

$$\forall b, b' \in \mathcal{B} \text{ such that } b' > b,$$

$$\sqrt{(x_{b'} - x_b)^2 + (y_{b'} - y_b)^2} + N\beta_{b,b'} \geq \frac{\kappa}{2}\left(\sum_{w\in\mathcal{W}} W_w\omega_{b,w} + \sum_{w\in\mathcal{W}} W_w\omega_{b',w}\right) \tag{41}$$

Variables: $\alpha_{s,b}, \omega_{b,w}, \rho_{b,r}, \beta_{b,b'}, \gamma_{b,b',u} \in \{0,1\}$, $x_b, y_b \in \mathbb{R}$

For each beam $b \in \mathcal{B}$, we introduce beam center variables $(x_b, y_b) \in \mathbb{R}^2$, beam diameter, satellite reflector and station allocation variables (respectively $\omega_{b,w}, \rho_{b,r}, \alpha_{s,b} \in \{0,1\}$ for all $w \in \mathcal{W}, r \in \mathcal{R}, s \in \mathcal{S}$) and corresponding "at most one" and "exactly one" constraints: (36), (37) and (38). They help write linearly the objective (35): covered traffic maximization. The proximity constraint that states that a station must be inside the disk of a beam to be covered by it is expressed in constraint (39). $M_s \in \mathbb{R}^+$ (precisely tuned) relaxes the constraints when $b \in \mathcal{B}$ does not cover $s \in \mathcal{S}$ ($\alpha_{s,b} = 0$). Constraints (40) force the $\beta_{b,b'} \in \{0,1\}$ variables to be equal to 0 if $b, b' \in \mathcal{B}$ ($b \neq b'$) use the same reflector. The antenna separation constraint occurs when two beams use the same reflector ($\beta_{b,b'} = 0$), equation (41) formulates that separation involving the Euclidean distance between the two beams, the mean of the two beam diameters and the proportionality coefficient κ.

The model (35) - (41) is non-linear because of constraints (39) and (41). However, thanks to *Proposition* 1 (approximation by $\mathcal{P}'$) and in the same way we did for the k-center problem in section 4, constraint (39) can be replaced by

$$\forall s \in \mathcal{S}, \forall b \in \mathcal{B}, \forall u \in \mathcal{U},$$

$$\begin{pmatrix} x_b - X_{\text{stations},s} \\ y_b - Y_{\text{stations},s} \end{pmatrix}^T \begin{pmatrix} U_{u,x} \\ U_{u,y} \end{pmatrix} \leq \frac{1}{2}\cos(\theta_{\max}) \sum_{w\in\mathcal{W}} W_w\omega_{b,w} + (1-\alpha_{s,b})M_s \tag{42}$$

In the same manner, constraint (41) can be replaced by a set of two constraints presented below :

$$\forall b, b' \in \mathcal{B} \text{ such that } b' > b, \quad \beta_{b,b'} + \sum_{u \in \mathcal{U}} \gamma_{b,b',u} \geq 1 \tag{43}$$

$\forall b, b' \in \mathcal{B}$ such that $b' > b, \forall u \in \mathcal{U}$,

$$\begin{pmatrix} x_{b'} - x_b \\ y_{b'} - y_b \end{pmatrix}^T \begin{pmatrix} U_{u,x} \\ U_{u,y} \end{pmatrix} \geq \frac{\kappa}{2} \left(\sum_{w \in \mathcal{W}} W_w \omega_{b,w} + \sum_{w \in \mathcal{W}} W_w \omega_{b',w} \right) - N(1 - \gamma_{b,b',u}) \tag{44}$$

The antenna separation constraints are activated in that case, first through constraints (43) that force at least one $\gamma_{b,b',u} \in \{0,1\}$ ($u \in \mathcal{U}$) to be equal to 1. Constraints (44) operate the separation according to *Proposition* 2 and coefficient κ when $\gamma_{b,b',u} = 1$ (approximation by $\mathcal{P}$). They are relaxed by $N \in \mathbb{R}^+$ when $\gamma_{b,b',u} = 0$.

6 Experiments

In addition to the fact that the new linearization scheme outperformed the one of [16] for large instances in our experiments (see Section 4), there are two other reasons in favor of choosing the new scheme instead of more classical linearizations. First, the separation constraint (41) has 2 variable points, the centers of beams b and b'. Hence, to follow the approach of [16], there would be 6 non linear terms to linearize (x_b^2, $x_{b'}^2$, $x_b x_{b'}$, y_b^2, $y_{b'}^2$ and $y_b y_{b'}$). Second, separation constraint (41) is non-convex, which was not addressed in [16]. Although using a linear combination of an under- and an over-estimated norm is likely to produce infeasible solutions, we nevertheless include the combinations (L_1, L_∞) and (CWD_{eu}, WtD_{isr}) [19]. Although the plane direction linearization scheme allows to model such combinations thanks to to properties established in Section 6.1, we found that the linearization was less efficient than the adhoc one. Hence we use this latter scheme to make the fairest comparison

6.1 Comparison of the proposed linearization with linear combination of norms

To compare the proposed linearization scheme with existing approximation we consider 10 instances of $N_S = 100$ stations, $N_B = 10$ beams, $N_R = 4$ stations a single beam diameter $W = 0.85$. The traffic demand distribution T_s is randomly generated between 1 and 200 while the fixed beam capacity is set to 500. We set $\kappa = \sqrt{3}$. We compare the linearizations based on 4, 8 and 12 plane directions (DIR2, DIR8 and DIR12) with natural linearizations of the (L_1, L_∞) and (CWD_{eu}, WtD_{isr}) linear combinations of norms (NL1LI and NWC) and the linearizations of these norms by the plane directions approach (DL1LI and DWC). We also design a MILP where the distance for proximity constraints (39) is over-estimated by the CWD_{eu} norm and the distance for separation constraints (41) is under-estimated by the WtD_{isr}) norm, both linearized in the natural way. This variant is named NWC*. Due to the property established in Section 3, NWC* has in theory the same approximation quality as the DIR8 MILP.

	est. traffic	real traffic	# viol ct (39)	# viol ct (41)
DIR4	3907,72	3907,72	0	0
DIR8	4336,132	4336,132	0	0
DIR12	4363,202	4363,202	0	0
NL1I	4105,987	3691,305	6,8	0,3
DL1I	4319,118	3510,509	14,4	0,7
NWC	3609,625	3423,058	3,4	0
DWC	3119,605	2797,824	5,8	0
NWC*	3802,439	3802,439	0	0

Table 4 Comparison of linearizations on the beam layout problem with a 500s CPU time limit

For the natural linearization of the non convex separation constraints L_1, L_∞, CWD_{eu} and WtD_{isr}, we need the introduction of additional binary variables. For the CWD_{eu} norm, three binary variables by pair (beam,stations) are needed to linearize the max, absolute x value and absolute y value operators. For the WtD_{isr} norm, one more binary variables by pair (beam,stations) is needed because of the global max operator. For L_1 and L_∞, two and three binary variables are needed for each pair (beam,station), respectively. In terms of number of binary variables this gives an advantage to the natural linearizations as none of them need more binary variables than the DIR4 linearization.

Table 4 gives for each MILP under a 500s time limit, the average estimated covered traffic on the 10 instances, the real average covered traffic, the average number of violated proximity constraints (39) and the average number of violated separation constraints (41). The estimated covered traffic correspond to the returned objective function. For the linear combination of norms, there may exist violated proximity and separation constraints. Hence for each violated proximity constraint between a station s and its assigned beam b (within a tolerance of $0.01W/2$), the traffic demand of s has to be subtracted from the total covered traffic. The real covered traffic is obtained by this process. The time limit of 500s was reached by each MILP on each instance.

The results show that the DIR12 MILP outperforms all other MILPs. The linear combination of norms L_1 and L_∞ (NL1I and DL1I) obtain an objective value close to the best value but there are so many violated proximity constraints that the real covered traffic is much lower. There are also violations of the separation constraints. The linear combination of norms CWD_{eu} and WtD_{isr} (NWC and DWC) obtains disappointing results. Even if there are much less violated proximity constraints and no violated separation constraints than for L1LI, the estimated covered traffic is lower than the DIR4 one. Notice that the natural linearizations obtain less constraints violations than the ones based on plane directions. The NWC* linearization obtains better results and there are no violated constraints, as expected but it stays slightly behind DIR4. Even if there are more binary variables in the linearizations based on place directions, the solver converges faster toward better solutions. For the experiments on larger and more complex instances, we consequently select the DIR linearizations.

6.2 Experiments on larger and more complex industrial instances

More experiments are conducted on larger and more complex instances issued from the industrial partner consisting of $N_S \in \{100, 200, 300\}$ user stations of fixed position, with the traffic demand distribution T_s being generated randomly in a realistic range: each draw defines an instance. The number of beams $N_B \in \{10, 20, 30\}$ grows with N_S. The number of reflectors has been set to $N_R = 4$, the number of diameters to $N_W = 2$ ($W_1 = 0.3^\circ$ and $W_2 = 0.5^\circ$), $\kappa = \sqrt{3}$. We tested different values of $n_{\text{directions}}$ to assess its impact on the numerical complexity: 10 instances were generated per number of user stations N_S considered, the resulting 30 instances being all tested on the numbers of discretized directions $n_{\text{directions}}$ in the set $[\![3;50]\!]$. The MILP solver used is Gurobi with a timeout per instance set to 180 seconds. Some other minor industrial constraints were integrated to the model but we chose not to discuss them here. The results are given in Fig. 6(a) in the form of relative gaps between best solution found and sum of traffic demands for the three types of instances tested. Each point of the three curves is an average gap value obtained over the 10 instances of the corresponding category of instances. As we could have predicted, the more beams and stations, the harder the convergence toward the optimal solution, materialized by higher average gaps in Fig. 6(a). Then, the main observation that can be made from these results is that, for a too low number of directions ($3 \leq n_{\text{directions}} \leq 8$), the approximation of the disks by $\mathcal{P}$ (separation constraint) and $\mathcal{P}'$ (proximity constraint) is too rough and does not allow to reach solutions of good quality. On the other hand, for a too high number of directions ($20 \leq n_{\text{directions}} \leq 50$), the gain in approximation accuracy becomes so small that the solution quality improvements, if any, do not compensate the increase in numerical complexity due to the growing model size: this explains the degradation of the average gaps in Fig. 6(a) for these values of $n_{\text{directions}}$. This is a general rule to keep in mind for applying this Euclidean norm linearization technique.

For illustration purposes, Fig. 6(b) is an example of instance that has been solved optimally with $N_S = 200$ and $N_B = 20$ (this particular optimum was reached with $n_{\text{directions}} = 12$ in less than 1500s). The user stations are represented by black dots covered by the 20 beams. Each beam color corresponds to a different satellite reflector antenna. Note that only one beam uses the smallest diameter W_1, all the others use W_2. Prior to using the proposed MILP approach, obtaining such a solution was out-of-reach for the industrial partner.

7 Concluding remarks

We introduced a general methodology based on MILP for linearizing inequality constraints involving the L_2 norm, even in the case of non convex constraints. This methodology allows to obtain both under- and over estimations under the same framework. We also showd that the L_1, L_∞, the euclidean Chamfering weighted distance in 2-D, and the Inverse square root weighted t-cost distance in 2-D correspond to particular cases of the proposed linearization and their linear combinations can also be expressed directly. The quality of the approximation is demonstrated on an opti-

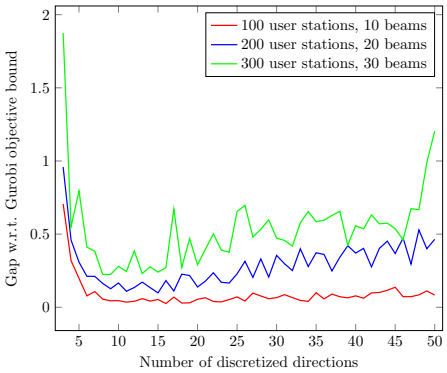

(a)

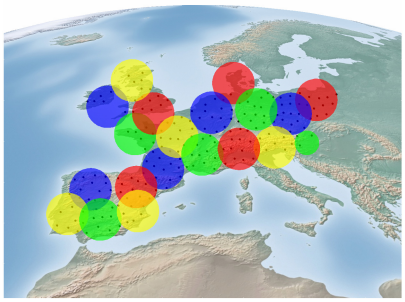

(b)

Fig. 6 (a) Campaign of runs for varying numbers of discretized directions and varying numbers of user stations (b) Example of instance with 200 user stations solved optimally with 12 discretized directions

mization problem involving euclidean distance: the continuous k-center problem. The computational experiments indeed showed the efficiency and the competitiveness of the proposed method that outperform other linearization techniques. We finally validated this approach on the beam layout problem, a crucial industrial problem for satellite manufacturers, for which we have reached significantly improved solutions compared to the existing hand-crafted ones. The proposed MILP also outperforms standard linearizations of existing approximations of the L_2 norm on this problem. Furthermore, we exhibit in this example that a minimum number of directions is required to obtain good quality solutions. Nevertheless, it is inappropriate to over approximate by considering a too high number of directions. In the latter case, the quality improvements of the solution will not counterbalance the increasing the numerical complexity. It seems that the tradeoff lives between 10 and 20 directions in the cases we encountered so far. The next steps, that are already a work in progress, will consist in improving the current model to remove symmetries and solve even larger instances, for finally benchmarking the methodology with MINLP solvers.

References

1. C. D'Ambrosio ans L. Liberti. Distance geometry in linearizable norms. In *Geometric Science of Information*, pages 830–837. Springer International Publishing, 2017.
2. A. Ben-Tal and A. Nemirovski. On polyhedral approximations of the second-order cone. *Mathematics of Operations Research*, 26(2):193–205, 2001.
3. P. Biswas and Y. Ye. Semidefinite programming for ad hoc wireless sensor network localization. *Third International Symposium on Information Processing in Sensor Networks*, pages 46–54, 2004.
4. M. Bousquet and G. Maral. *Satellite Communications Systems : Systems, Techniques and Technology*. Wiley, 5th edition, December 2009.
5. J.-T. Camino, C. Artigues, L. Houssin, and S. Mourgues. A greedy approach combined with graph coloring for non-uniform beam layouts under antenna constraints in multibeam satellite systems. *Advanced Satellite Multimedia Systems Conference and the 13th Signal Processing for Space Communications Workshop (ASMS/SPSC)*, 2014.
6. J.-T. Camino, C. Artigues, L. Houssin, and S. Mourgues. Mixed-integer linear programming for multibeam satellite systems design: Application to the beam layout optimization. In *2016 Annual IEEE Systems Conference (SysCon)*, 2016.
7. M. Celebi, F. Celiker, and H. Kingravi. On euclidean norm approximations. *Pattern Recognition*, page 278–283, 2011.
8. JM Cook. Rational formulae for the production of a spherically symmetric probability distribution. *Mathematics of Computation*, 11(58):81–82, 1957.
9. T Erber and G.M. Hockney. Equilibrium configurations of n equal charges on a sphere. *Journal of Physics A: Mathematical and General*, 24(23):L1369, 1991.
10. H. A Fayed and A. F Atiya. A mixed breadth-depth first strategy for the branch and bound tree of euclidean k-center problems. *Computational Optimization and Applications*, 54(3):675–703, 2013.
11. C. Gentile. Sensor location through linear programming with triangle inequality constraints. *IEEE Conf. on Communications*, pages 3192–3196, 2005.
12. F. Glineur, R. De Houdain, and B. Mons. Computational experiments with a linear approximation of second-order cone optimization, 2000. Image Technical Report 0001, Mons.
13. R. Harman and V. Lacko. On decompositional algorithms for uniform sampling from n-spheres and n-balls. *Journal of Multivariate Analysis*, 101(10):2297–2304, 2010.
14. K. Kiatmanaroj, C. Artigues, L. Houssin, and F. Messine. Frequency assignment in a SDMA satellite communication system with beam decentring feature. *Computational Optimization and Applications*, 56:439–455, 2013.
15. L. Liberti, C. Lavor, N. Maculan, and A. Mucherino. Euclidean Distance Geometry and Applications. *SIAM Review*, 56(1):3–69, 2014.
16. L. Liberti, N. Maculan, and Y. Zhang. Optimal configuration of gamma ray machine radiosurgery units: the sphere covering subproblem. *Optimization Letters*, v. 3, n. 1:109–121, 2009.
17. G. Mao, B. Fidan, and B. D. O. Anderson. Wireless sensor network localization techniques. *Elsevier/ACM Computer Networks*, pages 2529–2553, 2007.
18. N. Megiddo and K. J. Supowit. On the complexity of some common geometric location problems. *Society for Industrial and Applied Mathematics - SIAM J. COMPUT.*, 13(1):182–196, February 1984.
19. J. Mukherjee. Linear combination of norms in improving approximation of euclidean norm. *Pattern Recognition Letters*, pages 1348–1355, 2013.
20. M. E Muller. A note on a method for generating points uniformly on n-dimensional spheres. *Communications of the ACM*, 2(4):19–20, 1959.
21. MJ Peake, J Trevelyan, and G Coates. The equal spacing of n points on a sphere with application to partition-of-unity wave diffraction problems. *Engineering Analysis with Boundary Elements*, 40:114–122, 2014.
22. H. M. Rabie, I. A. El-Khodary, and A. A. Tharwat. A particle swarm optimization algorithm for the continuous absolute p-center location problem with euclidean distance. *International Journal of Advanced Computer Science and Applications (IJACSA)*, 4, 2013.
23. W. F. Riedl and B. Zönnchen. The k-center problem. *https://www-m9.ma.tum.de/games/kcenter-game/*. Last consulted on January 4, 2019.
24. E. B. Saff and A. B. J. Kuijlaars. Distributing many points on a sphere. *The mathematical intelligencer*, 19(1):5–11, 1997.
25. A. Sutou and Y. Dai. Global optimization approach to unequal sphere packing problems in 3d. *Journal of Optimization Theory and Applications*, 114:671–694, 2002.

26. G. Xue, J. B. Rosen, and P. M. Pardalos. A polynomial time dual algorithm for the euclidean multifacility location problem. *Proceedings of Second Conference on Integer Programming and Combinatorial Optimization*, pages 227–236, 1992.
27. G. Xue and Y. Yue. An efficient algorithm for minimizing a sum of euclidean norms with applications. *SIAM J. Optim.*, 7:1017–1036, 1997.